g-matrix calculations in finite hypernuclei

Dean Halderson
Physics Department, Western Michigan University, Kalamazoo, Michigan 49008
(Received 31 August 1992; revised manuscript received 29 March 1993)

g-matrix calculations have been performed for ${}^{5}_{\Lambda}$He, ${}^{17}_{\Lambda}$O, and ${}^{41}_{\Lambda}$Ca by solving the Λ-Σ coupled channels Bethe-Goldstone equation. The potentials employed were the Nijmegen model D and Nijmegen soft core. Calculations were performed with various choices for the Pauli-forbidden space and the energy denominator. The Nijmegen model D does a reasonable job of reproducing most experimental single-particle energies, but the calculated ground-state binding energies vary smoothly from being underbound in the ${}^{5}_{\Lambda}$He to overbound in ${}^{41}_{\Lambda}$Ca. The Nijmegen soft core underbinds all single Λ states, but gives level spacings which agree with experimental values.

PACS number(s): 21.80.+a

I. INTRODUCTION

Earlier calculations [1,2] have developed effective potentials for the ΛN and ΣN interactions from realistic two-baryon potentials [3–5]. These calculations were based on solutions for the hyperon single-particle energies in nuclear matter via first-order Brüeckner calculations. An effective interaction was extracted from momentum-averaged solutions to the Bethe-Goldstone equation. This effective interaction is a function of nuclear density. At first, predictions for lambda single-particle energies in finite nuclei were made by selecting an appropriate density and solving the Hartree equations with the resulting ΛN interaction. Later, density dependent Hartree calculations were performed [6].

In this paper we omit the intermediate step of a nuclear matter calculation and perform the Brüeckner calculation for finite Λ hypernuclei as was done in the original work of Bandō [7]. This procedure eliminates the need to choose a density for each single-particle state, and, therefore, should provide a more direct means of determining whether a specified two-baryon interaction, fit to two-body data, can reproduce observed Λ single-particle energies.

The calculation employs the reference spectrum method to produce *g*-matrix elements for the Nijmegen model D [3,4] and Nijmegen soft core (NSC) [5] potentials. Pauli corrections were performed in a *jj*-coupled basis. Use of a Brüeckner Q and kinetic energy propagator produced reasonable agreement with the lambda single-particle energies for model D. Exceptions were the ${}^{5}_{\Lambda}$He and ${}^{41}_{\Lambda}$Ca ground states. Agreement for ${}^{5}_{\Lambda}$He was poor because the calculations ignored the center-of-mass (c.m.) kinetic energy and Hartree self-consistency for the Λ single-particle wave functions. These two effects were investigated by fitting an effective interaction to Pauli-corrected relative *g*-matrix elements at a specified starting energy. The Hartree self-consistency could then be sought in the Λ-nucleus center-of-mass coordinate system. The final results indicate that ${}^{17}_{\Lambda}$O and ${}^{41}_{\Lambda}$Ca $0p$ and $1s$-$0d$ calculated levels were in reasonable agreement with experimental results; however, ${}^{5}_{\Lambda}$He is underbound by approximately 1.1 MeV and the ${}^{41}_{\Lambda}$Ca ground state overbound by 5 MeV. The same procedure for the NSC leads to reasonable spacings between single-particle energies, but a consistent underbinding of them all.

II. PROCEDURE

We follow Ref. [7] to extend Brüeckner-Goldstone theory from finite nuclei to finite hypernuclei and obtain a diagonal lambda single-particle potential for hole states of Hartree form,

$$\langle \Lambda | U | \Lambda \rangle = \sum_N \langle \Lambda N | g(\omega = \epsilon_\Lambda + \epsilon_N) | \Lambda N \rangle \ . \tag{1}$$

The particle-hole single-particle potential will be defined as

$$\langle \Lambda | U | \lambda \rangle = \sum_N \langle \Lambda N | g(\omega = \epsilon_\Lambda + \epsilon_N) | \lambda N \rangle \ , \tag{2}$$

thereby canceling the second-order diagrams in Fig. 1. This also includes the possibility of a sigma as an excited lambda state, and the $\Lambda\Sigma$ single-particle coupling potential becomes

$$\langle \Lambda | U | \Sigma \rangle = \sum_N \langle \Lambda N | g(\omega = \epsilon_\Lambda + \epsilon_N) | \Sigma N \rangle \ . \tag{3}$$

Therefore, the three-body diagram in Fig. 2(a) is included in those canceled by the single-particle potential

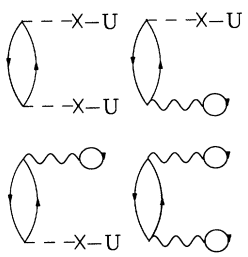

FIG. 1. Second-order diagrams canceled by the definition of the single-particle potential.

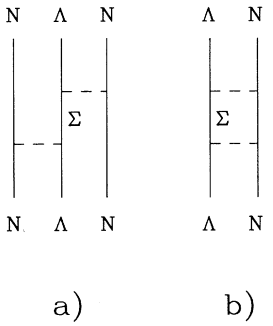

FIG. 2. (a) A three-body diagram. (b) A dispersive diagram.

prescription. The particle-particle single-particle potential is defined in analogy with the Hartree definition of the hole-hole potential:

$$\langle\lambda|U|\lambda\rangle=\sum_{N}\langle\lambda N|g(\omega=\epsilon_\lambda+\epsilon_N)|\lambda N\rangle\ . \tag{4}$$

Since the ΛN interaction has approximately one-half the strength of the NN interaction and with the cancellation of the second-order diagrams, one would expect the first-order Goldstone diagram in Fig. 3(a) to provide a reasonably good approximation to the lambda ground-state energy. This diagram, when expanded to show one of its contributions as in Fig. 3(b), contains intermediate Σ states. Therefore, the corresponding Bethe-Goldstone equation,

$$\Psi=\Phi+\frac{Q}{e}v\Psi\ , \tag{5}$$

contains a correlated wave function with lambda and sigma components,

$$\Psi=\begin{bmatrix}\Psi_\Lambda\\ \Psi_\Sigma\end{bmatrix}\ .$$

For the present the energy denominator,

$$e=\begin{bmatrix}e_\Lambda & 0\\ 0 & e_\Sigma\end{bmatrix}\ ,$$

will be taken to be

$$e=\begin{bmatrix}\omega-T & 0\\ 0 & \omega-T-\Delta mc^2\end{bmatrix}\ ,$$

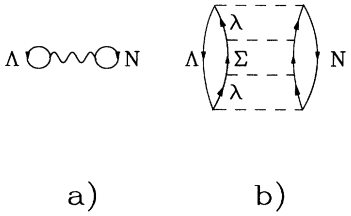

FIG. 3. (a) The first-order Goldstone diagram. (b) A contributor to the first-order Goldstone diagram.

where $\Delta m=m_\Sigma-m_\Lambda$, and T is the kinetic energy of the intermediate pair.

In this work it is assumed that oscillator wave functions approximate the nuclear wave functions, and the oscillator constant, $b^2=\hbar/m_N\Omega$, is chosen to reproduce the nuclear core size. Values of $b=1.394$, 1.791, and 1.970 fm were used for ^{4}He, ^{16}O, and ^{40}Ca, respectively. It is also assumed that these orbits and the nuclear binding energies are not affected by the presence of the lambda. Tests were made which demonstrated that 5% changes in the nuclear radius produced relatively small changes in the calculated single-particle energies.

Initially, the lambda Hartree orbits will be taken to be oscillators with the same Ω. Calculation of the ls-coupled YN matrix elements proceeds in the usual fashion by performing an unequal-mass Talmi transformation [8] to the ΛN relative and c.m. coordinates, $|\phi_{nl}(r)\otimes\phi_{NL}(R)(\mathcal{L})\otimes S(J)\rangle$. Recoupling the spin to the relative wave function, one can define an uncorrelated wave function, $\Phi=|\phi_{nlSj}(r)\otimes\phi_{NL}(R)(J)\rangle$. The correlated wave function is defined in terms of the relative correlated wave function, $\Psi=|\psi(r)\otimes\phi_{NL}(R)(J)\rangle$. Operating on the left of Eq. (5) with $\langle\phi_{NL}(R)|$ and assuming that $T_{\text{c.m.}}=-[\hbar^2/2(m_N+m_\Lambda)]\nabla_R^2$ is diagonal in the $\phi_{NL}(R)$ basis, one obtains the relative Bethe-Goldstone equation

$$\psi(r)=\phi_{nlSj}(r)+\frac{Q}{\omega-(T_r+\epsilon_{NL}/2+\Delta mc^2\delta_{Y\Sigma})}v\psi(r)\ , \tag{6}$$

where $T_r=-(\hbar^2/2\mu_Y)\nabla_r^2$ and $\mu_Y=m_Ym_N/(m_Y+m_N)$. Operating on the left with $\omega-(T_r+\epsilon_{NL}/2+\Delta mc^2\delta_{Y\Sigma})$ and setting $Q=1$, one obtains a differential equation for the reference spectrum correlated wave function,

$$\begin{bmatrix}\omega-(\epsilon_{NL}/2+T_r) & 0\\ 0 & \omega-(\epsilon_{NL}/2+T_r+\Delta mc^2)\end{bmatrix}\begin{bmatrix}\psi_\Lambda\\ \psi_\Sigma\end{bmatrix}=\begin{bmatrix}\phi_\Lambda\\ 0\end{bmatrix}+v\begin{bmatrix}\psi_\Lambda\\ \psi_\Sigma\end{bmatrix}\ . \tag{7}$$

For sigma starting states $\begin{bmatrix}\phi_\Lambda\\ 0\end{bmatrix}$ is replaced by $\begin{bmatrix}0\\ \phi_\Sigma\end{bmatrix}$, where ϕ_Σ is chosen to have the same $b_{\text{rel}}^2=\hbar/\mu_\Lambda\Omega$ relative oscillator constant. For $l\neq j$,

$$\psi_Y=\frac{u_Y(r)}{r}Y_{l_<1j}+\frac{w_Y(r)}{r}Y_{l_>1j}\ . \tag{8}$$

For $l=j$,

$$\psi_Y=\frac{u_Y(r)}{r}Y_{l0l}+\frac{w_Y(r)}{r}Y_{l1l}\ , \tag{9}$$

since the antisymmetric spin-orbit force couples $S=0$ and $S=1$ channels. Four coupled second-order differential equations are obtained from Eq. (8) by multiplying from the left by $(Y^+_{l_<1j}0)$, $(Y^+_{l_>1j}0)$, $(0\,Y^+_{l_<1j})$, and $(0\,Y^+_{l_>1j})$, integrating over the angular variables, and taking the expectations of the spin variables. Four coupled, second-order differential equations are also obtained from Eq. (9) by the corresponding operations. The four coupled equations are solved by applying the boundary con-

ditions that $\psi \to 0$ at the core radius and that as $r \to \infty$ each component of ψ approaches the solution obtained when v is set equal to zero. The large component of ψ will then heal to the uncorrelated relative wave function.

Once the correlated relative wave functions are available, reference spectrum relative g-matrix elements are constructed by integrating from the core radius to infinity:

$$\langle \phi_{nlSj}(Y)|g|\phi_{n'l'S'j}(Y')\rangle = \int\int_{a_c}^{\infty} \phi^{+}_{nlSj}(Y) v \psi_{n'l'S'j'}(Y') r^2 dr\, d\Omega_r - \frac{\hbar^2}{2\mu_Y}\left[u^{\rm osc}_{nlSj}(Y)\frac{dz_{n'l'S'j}(Y)}{dr}\right]_{a_c}, \tag{10}$$

where z is u or w.

Matrix elements in the jj-coupling scheme,

$$\langle \phi_{n_Y l_Y j_Y}(r_Y)\phi_{n_N l_N j_N}(r_N)(J)|g_r|\phi_{n'_Y l'_Y j'_Y}(r_{Y'})\phi_{n'_N l'_N j'_N}(r_N)(J)\rangle$$

are then reconstructed. The Pauli operator, Q, is now reinstated by solving the correction equation by matrix operation,

$$g = g_r + g_r\left[\frac{Q}{e} - \frac{1}{e}\right]g, \tag{11}$$

in the jj-coupled basis. A Brüeckner Q is employed so that both intermediate particles must be above the Fermi sea to make $Q=1$. Even though the $0s_{1/2}(\Lambda)$ state is only half filled, the lambda Fermi energy is taken to be $\epsilon_{F\Lambda} = 2n_\Lambda + l_\Lambda = 0$. The choice $\epsilon_{F\Lambda} < 0$, as employed in Ref. [6], decreases the calculated lambda single-particle energies by $\frac{1}{2}$ to 1 MeV. The correction operation converges very rapidly with total principle quantum number and a value of $N_m = 2n_\Lambda + l_\Lambda + 2n_N + l_N \leq 6$ is adequate for all calculations with model D. The NSC required $N_m = 8$ for ${}^{41}_{\Lambda}$Ca. Finally, the lambda single-particle energies are expressed in terms of the jj-coupled matrix elements,

$$\epsilon_\Lambda = \langle \phi_{n_\Lambda l_\Lambda j_\Lambda}|T|\phi_{n_\Lambda l_\Lambda j_\Lambda}\rangle + \sum_{J,(n_N l_N j_N)} 2\frac{(2J+1)}{(2j_\Lambda+1)}\langle \phi_{n_\Lambda l_\Lambda j_\Lambda}\phi_{n_N l_N j_N}(J)|g(\omega = \epsilon_\Lambda + \epsilon_N)|\phi_{n_\Lambda l_\Lambda J_\Lambda}\phi_{n_N l_N j_N}(J)\rangle . \tag{12}$$

The nucleon single-particle energies in this equation are taken from experiment and are listed in Table I.

The baryon-baryon potentials employed in Eq. (5) are the Nijmegen model D as given in Ref. [3] and the NSC as given in Ref. [5]. The interaction is made to be charge symmetric by setting the neutron mass equal to the proton mass. The potential is in the form

$$V = V_c + V_\sigma \sigma_1\cdot\sigma_2 + V_T S_{12} + V_{so} L\cdot S + V_Q Q_{12} + V_{soa}\tfrac{1}{2}(\sigma_1 - \sigma_2)\cdot L , \tag{13}$$

where

$$S_{12} = 3(\sigma_1\cdot\hat{r})(\sigma_2\cdot\hat{r}) - (\sigma_1\cdot\sigma_2) ,$$

$$Q_{12} = \tfrac{1}{2}[(\sigma_1\cdot L)(\sigma_2\cdot L) + (\sigma_2\cdot L)(\sigma_1\cdot L)] .$$

III. RESULTS

We begin with model D. The effect of Pauli corrections for this potential are shown in Fig. 4 for ${}^{17}_{\Lambda}$O. The dashed lines are the results of including only the lambda sector for the matrix operations in Eq. (11), and the solid lines are the results when both the lambda and sigma sectors are included. The first column shows the $Q=1$ results, the second when $\epsilon_{F\Lambda} = \epsilon_{FN} = 0$, the third when $\epsilon_{F\Lambda} = 0$, $\epsilon_{FN} = 1$, the fourth when $\epsilon_{F\Lambda} = 0$, $\epsilon_{FN} = 2$. Column three would be the correct choice for ${}^{17}_{\Lambda}$O. The Pauli corrections are one source of nucleus dependence (or density dependence in the case of an effective interaction) for the g-matrix elements, and this figure demonstrates that the effect is not large for model D.

In Fig. 5 are the results of five calculations for the lambda single-particle energies in ${}^{5}_{\Lambda}$He (dot-dashed lines), ${}^{17}_{\Lambda}$O (dashed lines), and ${}^{41}_{\Lambda}$Ca (solid lines). The first column shows the energies when only the ΛN interaction is used and when the ΛN reduced mass is replaced with the NN reduced mass in the Bethe-Goldstone equation. The second column is the same as the first except that the ΛN reduced mass is reinstated. This produces an approximately 5 MeV reduction in the single-particle energies. The third column is the same as the second except that an oscillator potential was added to the energy denominator, $e_Y \to \omega - (H_{\rm osc} + \Delta mc^2\delta_{Y\Sigma})$. This produces a 1 to 2 MeV increase in the energies and demonstrates the effect

TABLE I. Table I. Nucleon single-particle energies (MeV).

	$0s_{1/2}$	$0p_{3/2}$	$0p_{1/2}$	$0d_{5/2}$	$1s_{1/2}$	$0d_{3/2}$
^{4}He	−19.8					
^{16}O	−38.0	−21.8	−15.7			
^{40}Ca	−56.7	−48.5	−36.5	−22.6	−18.2	−15.6

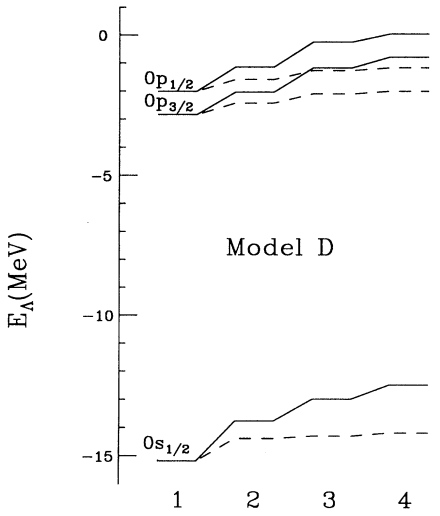

FIG. 4. Calculated single-particle energies for $^{17}_{\Lambda}$O with model D. The dashed lines correspond to Pauli corrections performed only in the lambda space; the solid lines correspond to Pauli corrections performed in the full lambda plus sigma space.

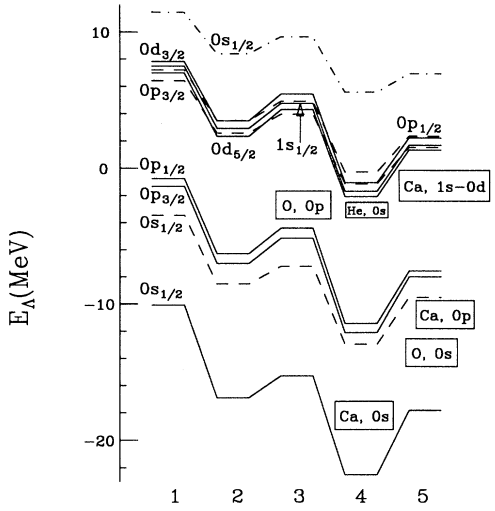

FIG. 5. Calculated single-particle energies. The dot-dashed line is for $^{5}_{\Lambda}$He, the dashed lines for $^{17}_{\Lambda}$O, and the solid lines for $^{41}_{\Lambda}$Ca. The first column shows the energies when only the ΛN interaction is used and when the ΛN reduced mass is replaced with the NN reduced mass in the Bethe-Goldstone equation. The second column is the same as the first except that the ΛN reduced mass is reinstated. The third column is the same as the second except that an oscillator potential was added to the energy denominator. The fourth column is the same as the second except that coupling to the sigma channels is now included. The fifth column is the same as the fourth except that the contribution of an individual nucleon orbit is multiplied by its partial occupation probability.

of the choice of a particle-particle, single-particle spectrum. The fourth column is the same as the second except that coupling to the sigma channels is now included. The coupling produces a 4 to 6 MeV drop in the energies. The fifth column is the same as the fourth except that the contribution of an individual nucleon orbit is multiplied by its partial occupation probability (POP) as determined in Ref. [9]. This gives the prescription

$$\langle \Lambda | U | \Lambda \rangle \rightarrow \sum_N \langle \Lambda N | g(\omega = \epsilon_\Lambda + \epsilon_N) | \Lambda N \rangle P_N \qquad (14)$$

for the lambda single-particle energies. This calculation was included to demonstrate that the inclusion of partial occupation probabilities, at least in this approximation, shifts the energies up, but, like the change to an oscillator denominator, does not change the relative spacings significantly.

The fourth column represents the final prediction of the procedure described above. To this point the present calculation gives the same result as Ref. [6]. Small differences are due to the choice of oscillator constants and Pauli-forbidden space for the Λ. (Reference [6] allows the Λ to rescatter into the 0s state.) Experimental values, as extracted from the curve in Fig. 7 of Ref. [10], are included in this figure as boxes which have heights approximately equal to estimated error bars. Agreement with the experimental points is generally good. Exceptions are the $^{5}_{\Lambda}$He and $^{41}_{\Lambda}$Ca ground states. A possible source of discrepancy is the use of Eq. (12). This prescription for the single-particle energies is certainly in error in that it does not include corrections for the c.m. kinetic energy. Another possible source is the failure to apply the Hartree condition to the lambda single-particle orbits. Both of these effects are expected to be large for $^{5}_{\Lambda}$He.

In order to incorporate both the Hartree condition and c.m. corrections into the calculation it will be necessary to eliminate the dependence of the g-matrix elements on the c.m. coordinate of the two interacting particles. Therefore, an effective interaction has been constructed. Several steps are necessary to develop this interaction. They are demonstrated in Table II.

First, a test is made to determine the adequacy of an "average-angle Q." Here one makes Pauli corrections in the space of relative g-matrix elements with the condition that $Q=1$ for $2n_Y+l_Y+2N_Y+L_Y \geq N^Y_{\max}$ and then constructs the jj-coupled matrix elements. A comparison of the first column of Table II, which is the same as column four in Fig. 5, and the second column of Table II, which employs the average-angle Q, demonstrates that the average-angle Q does a reasonable job of reproducing the original calculations. For this column $N^\Lambda_{\max}=N^\Sigma_{\max}=2$ for $^{5}_{\Lambda}$He and $^{17}_{\Lambda}$O, and $N^\Lambda_{\max}=N^\Sigma_{\max}=3$ for $^{41}_{\Lambda}$Ca.

Second, the average-angle calculation is repeated, but with all values of ϵ_{NL} set equal to $\frac{3}{2}\hbar\omega$ for $^{5}_{\Lambda}$He, and $\frac{5}{2}\hbar\omega$ for $^{17}_{\Lambda}$O and $^{41}_{\Lambda}$Ca. Column three of Table II shows that the effect of a constant c.m. energy is small. However, the third step consists of evaluating all relative matrix elements at a constant starting energy. Values of $\omega=-33$ and -40 MeV were used for $^{17}_{\Lambda}$O and $^{41}_{\Lambda}$Ca, respectively. Column four of Table II shows that this produced a spreading of the single-particle energies within an individual hypernucleus. It is this starting energy

TABLE II. Lambda single-particle energies (MeV).

	1	2	3	4	5	6	7
$^{5}_{\Lambda}$He($0s_{1/2}$)	5.3	6.1	6.1	6.1	6.9	−1.1	−1.1
$^{17}_{\Lambda}$O($0s_{1/2}$)	−13.2	−13.4	−13.5	−14.4	−13.8	−14.8	−14.9
$0p_{3/2}$)	−1.4	−1.6	−1.8	−1.2	−1.1	−2.7	−2.8
$0p_{1/2}$)	−0.5	−0.7	−0.9	−0.2	−0.1	−1.9	−1.8
$^{41}_{\Lambda}$Ca($0s_{1/2}$)	−22.7	−23.2	−22.9	−25.9	−27.0	−27.9	−27.8
($0p_{3/2}$)	−12.3	−12.7	−12.6	−13.5	−14.7	−15.0	−15.1
($0p_{1/2}$)	−11.7	−12.0	−11.9	−12.7	−13.9	−14.2	−14.1
($0d_{5/2}$)	−2.3	−3.0	−2.8	−2.2	−3.3	−4.0	−4.1
($1s_{1/2}$)	−1.9	−2.7	−2.3	−1.9	−3.2	−4.5	−4.5
($0d_{5/2}$)	−1.3	−2.0	−1.7	−1.1	−2.2	−2.9	−2.8

dependence, and to a lesser extent the Pauli corrections, that prevents one effective interaction from reproducing the results of the complete calculation for the heavier systems with model D. No such difficulty occurs in $^{5}_{\Lambda}$He, since there is only one starting energy.

A set of relative g-matrix elements, free of ϵ_{NL} and starting energy dependence, is now available for determining an effective interaction for each nucleus. The $^{17}_{\Lambda}$O matrix elements were fit to a sum of three Yukawa potentials,

$$V^k=\sum_{i=1}^{3} V_i^k \exp(-x_i)/x_i \ , \tag{15}$$

where $x_i=r/r_i$. The ranges are $r_1=0.3$, $r_2=0.4$, and $r_3=0.6$ fm. A limit of $|V_i^k| \leq 10\,000$ MeV was invoked to ease the numerical accuracy requirements. This restriction did cause some difficulty in simultaneously fitting both s and d waves of the central interaction. The parameters of the fit are shown in Table III.

The results for the single-particle energies, calculated with the effective interaction, are shown in column five of Table II and agree well with column four for $^{17}_{\Lambda}$O. They also agree reasonably well for $^{5}_{\Lambda}$He and $^{41}_{\Lambda}$Ca, again demonstrating that the Pauli corrections were not strongly nucleus dependent for model D. The effective interaction should, therefore, be quite good throughout the p shell. The effective interaction results do, of course, produce similar spreading of the single-particle energies as was found for the constant starting energy calculation.

The effective interaction can now be used in a calculation that eliminates the c.m. kinetic energy and satisfies the Hartree self-consistency. The method employed is that of Ref. [11] and involves a transformation to the coordinate that locates that lambda relative to the c.m. of the nuclear core. A comparison of columns five and six indicates that the Hartree condition and proper treatment of the center of mass produces a lowering of the $^{17}_{\Lambda}$O $0s_{1/2}$ state by 0.9 MeV. Including this change in the fourth column of Fig. 5, one obtains a final, calculated value of 13.9 MeV, slightly below the experimental results. Continuing in a similar manner, one obtains a final,

TABLE III. Effective interaction parameters (MeV).

	V_1	V_2	V_3
Triplet even	9999.977	−4969.260	86.035
Triplet odd	9999.971	−3753.200	71.729
Singlet even	10 000.003	−4248.739	−149.542
Singlet odd	6545.115	−3270.224	96.832
Spin-orbit even	−597.176	−271.174	21.824
Spin-orbit odd	−623.715	−502.359	40.280
Tensor even	2152.507	−1225.345	63.625
Tensor odd	−144.196	−40.400	33.600
Antisymmetric spin-orbit even	460.514	−9.999	0.0
Antisymmetric spin-orbit odd	460.514	−9.999	0.0
Triplet quadratic spin-orbit even	−299.589	36.007	0.0
Triplet quadratic spin-orbit odd	−42.538	52.542	−4.721
Singlet quadratic spin-orbit even	299.589	−36.007	0.0
Singlet quadratic spin-orbit odd	42.538	−52.542	4.721

calculated value for the $^{17}_{\Lambda}$O $0p$ states in agreement with experiment, final, calculated values for the $^{41}_{\Lambda}$Ca $0d$ and $0p$ states approximately 1 MeV below the experimental values, and a final, calculated value for the $^{41}_{\Lambda}$Ca $0s$ state approximately 5 MeV below the experimental value. A similar result was obtained in Ref. [7] using a density dependent Hartree procedure. However the conclusion that model D overbinds the $^{41}_{\Lambda}$Ca ground state differs from the conclusion in Ref. [6]. With POP and improved single-particle wave functions the final $^{41}_{\Lambda}$Ca single-particle energies agree with experimental values. The source of the discrepancy is the method employed to improve the single-particle wave function. Both methods rely on expanding the wave function in terms of oscillator wave functions, but the method employed in the present paper removes the c.m. excitations from the wave functions.

The center-of-mass correction is so large for $^{5}_{\Lambda}$He that one needs to iterate the single-particle energy calculation and effective interaction fit instead of making the simple adjustment of the last paragraph. When this is done, one obtains a final result of -2.0 ± 0.2 MeV, with the uncertainty due to the effective interaction fit. This value is 1.1 MeV above the experimental result of -3.14 MeV.

Also included in Table II are the results from the hyperon Nijmegen Gaussian (YNG) effective interaction from Ref. [1]. Column seven shows the results with the choice $k_F=1.12$ fm^{-1} and $\chi=0$. These values demonstrate that it is possible to select one Fermi momentum for the YNG interaction that closely approximates the results from the present effective interaction. It also demonstrates the uncertainty involved in choosing a Fermi momentum. In Ref. [1] the $^{5}_{\Lambda}$He calculation was performed at $k_F=0.9$ fm^{-1} to yield a value of -3.07 MeV. This would lead one to assume that the Nijmegen model D correctly binds $^{5}_{\Lambda}$He, whereas it underbinds the system when one employs the kinetic energy propagator.

The same techniques were then applied to the NSC. Although the phase shift fits in Ref. [5] did not include the antisymmetric spin-orbit interaction, it is included here with the form factor Λ_{27+8_s}. This produces an antisymmetric spin-orbit interaction of size similar to model D. A comparison equivalent to column four of Fig. 5 is shown for model D and the NSC in the first two columns of Fig. 6. The NSC underbinds all levels, but gives level spacings, both within a nucleus and between nuclei, that agree with experimental spacings. In fact, if one makes the c.m. and Hartree consistency corrections to the single-particle energies, they are all approximately 4 MeV high, as shown in the third column of Fig. 6. The means by which the NSC accomplished this feat is through the $\Lambda\Sigma$ coupling.

In Fig. 7 is shown the equivalent of Fig. 1 for the NSC. Here one sees that the Pauli corrections are very large when the appropriate ΣN states are eliminated from the forbidden space. The corrections are large because the $\Lambda\Sigma$ coupling for the NSC is very large—about twice that for model D. This strong coupling was demonstrated in Ref. [2] where the NSC produced a large width for the Σ in nuclear matter. In finite nuclei the two-body matrix elements become very Fermi-energy, and hence nucleus,

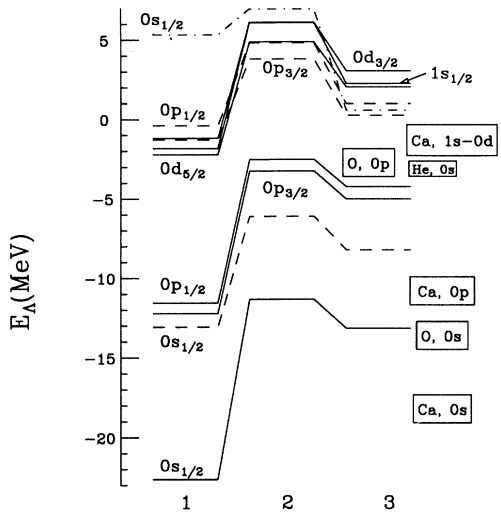

FIG. 6. Calculated single-particle energies. The dot-dashed line is for $^{5}_{\Lambda}$He, the dashed lines for $^{17}_{\Lambda}$O, and the solid lines for $^{41}_{\Lambda}$Ca. The first column is for model D, the second for the soft core, and the third includes c.m. and Hartree condition corrections to the wave functions for the soft core.

dependent. The $|0s(\Lambda)0s(N),S=1\rangle$ diagonal matrix element, for instance, weakens very rapidly as the forbidden space is enlarged. Hence, the Pauli corrections to the dispersive diagrams, shown in Fig. 2(b), give rise to much of the density dependence of an equivalent effective interaction for the NSC.

In Ref. [2] it was demonstrated that a change in the energy denominator could produce better binding energies for the NSC. The kinetic energy propagator was replaced with one that included the single-particle potential, $\omega-T\rightarrow\omega-(T+U)$. We have attempted a similar substitution for finite nuclei. This raises the question of how one chooses a particle spectrum for the nucleons and

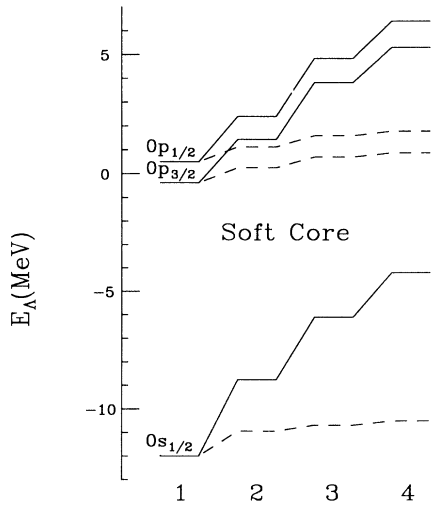

FIG. 7. Same as Fig. 4 for the soft core.

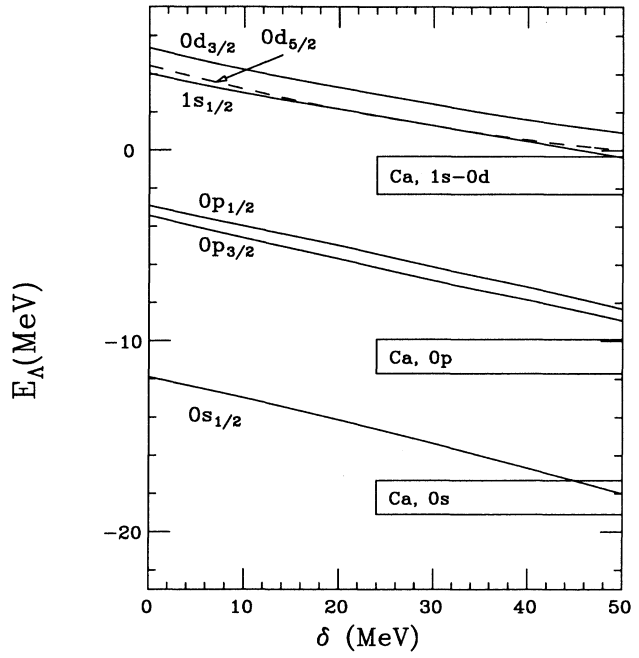

FIG. 8. Soft core results for $^{41}_{\Lambda}$Ca with shifted oscillator denominator as a function of the shift. Boxes represent approximate experimental results.

hyperons. There is no Hartree-Fock condition for a definition of the particle spectrum. Clearly, from Fig. 5, a change to a harmonic oscillator U moves the NSC results in the wrong direction. One could reason that since the hole spectrum is shifted downward from the oscillator spectrum with the Hartree-Fock condition, then U should be chosen so as to shift the particle spectrum downward. This particle spectrum shift was employed in early Brüeckner calculations [12]. Therefore, a shift δ was subtracted from the harmonic oscillator Hamiltonian to give a propagator, $1/[\omega-(T+U_{\rm osc}-\delta)]$. The $^{41}_{\Lambda}$Ca results, with the addition of the same c.m. and Hartree corrections used for Fig. 6, are plotted as a function of δ in Fig. 8. A value of $\delta=50$ MeV yields the experimental ground-state energy, and the level spacings are not unreasonable. However, we favor the $\delta=0$ calculations with the kinetic energy denominator for the following reason. A variational calculation [13] and a calculation with the Yakubovsky equations [14] gave ^{4}He binding energies of 22.9±0.5 MeV and 20.5 MeV, respectively, with the Reid potential, while a g-matrix calculation that includes $-U$ insertions in particle lines (approximated by our kinetic energy denominator) gave 19.5±2.0 MeV [15]. A similar result of −20.08 MeV was obtained in Ref. [16] when $-U$ insertions were included in the e^s formalism.

Therefore, the NSC, although not producing the correct binding energies with the kinetic energy propagator, has demonstrated a mechanism for obtaining reasonable single-particle energy spacings. One did not need to introduce a three-body interaction to obtain these level spacings.

IV. CONCLUSIONS

The lambda single-particle energies have been obtained for $^{5}_{\Lambda}$He, $^{17}_{\Lambda}$O, and $^{41}_{\Lambda}$Ca by solving the Λ-Σ coupled channels Bethe-Goldstone equation with the Nijmegen model D and soft core potentials. The final results for model D indicate that $^{17}_{\Lambda}$O calculated levels and $^{41}_{\Lambda}$Ca 0p and 1s-0d calculated levels were in reasonable agreement with experimental results. However, a trend of disagreement between the calculated and the experimental results is apparent in the ground-state binding energies. The ground-state energies go smoothly from underbound in the light system to overbound in the heavy system.

The soft core underbinds all levels, but produces reasonable level spacings both within a nucleus and between nuclei. The level spacing results are due to the strong ΛΣ coupling, primarily in the triplet even channel. Because this mechanism can reproduce the experimental level spacing, it appears very likely that a two-body YN potential can be constructed that fits not only scattering data, but also the experimental single-particle energies.

ACKNOWLEDGMENTS

This work was supported in part by the National Science Foundation under Grant No. PHYS-9202938. Thanks are also due to the Institute for Nuclear Theory at the University of Washington for its hospitality during the completion of this manuscript and to Th. A. Rijken for providing the soft core coordinate space code.

[1] Y. Yamamoto and H. Bandō, Prog. Theor. Phys. Suppl. **81**, 9 (1985).
[2] Y. Yamamoto and H. Bandō, Prog. Theor. Phys. Suppl. **83**, 254 (1990).
[3] M. M. Nagels, T. A. Rijken, and J. J. deSwart, Phys. Rev. D **12**, 744 (1975); **15**, 2547 (1977).
[4] M. M. Nagels, Ph.D. thesis, University of Nijmegen, 1975.
[5] P. M. M. Maessen, T. A. Rijken, and J. J. deSwart, Phys. Rev. C **40**, 2226 (1989).
[6] Y. Yamamoto, A. Reuber, H. Himeno, S. Nagata, and T. Mutoba, submitted to Czech. J. Phys.
[7] H. Bandō, Prog. Theor. Phys. **66**, 1349 (1981).
[8] L. Trlifaj, Phys. Rev. C **5**, 1534 (1972).
[9] R. L. Becker, Phys. Rev. Lett. **24**, 400 (1970).
[10] R. E. Chrien and C. B. Dover, Annu. Rev. Nucl. Part. Sci. **39**, 113 (1989).
[11] D. Halderson, Phys. Rev. C **30**, 941 (1984).
[12] H. S. Köhler and R. J. McCarthy, Nucl. Phys. **A106**, 313 (1967).
[13] J. Lomnitz-Adler, V. R. Pandharipande, and R. A. Smith, Nucl. Phys. **A361**, 399 (1981).
[14] J. A. Tjon, Phys. Rev. Lett. **40**, 1239 (1978).
[15] D. W. Halderson and P. Goldhammer, Phys. Rev. C **15**, 394 (1977).
[16] J. G. Zabolitzky, Nucl. Phys. **A228**, 285 (1974).